



Life-cycling and uncovering cation-trapping evidence of a monolithic inorganic electrochromic device: glass/ITO/WO₃/LiTaO₃/NiO/ITO

Dongmei Dong, Wenwen Wang, Aline Rougier, Guobo Dong, Mathias da Rocha, Lionel Presmanes, Khawla Zrikem, Giljoo Song, Xungang Diao, Antoine Barnabé

► To cite this version:

Dongmei Dong, Wenwen Wang, Aline Rougier, Guobo Dong, Mathias da Rocha, et al.. Life-cycling and uncovering cation-trapping evidence of a monolithic inorganic electrochromic device: glass/ITO/WO₃/LiTaO₃/NiO/ITO. *Nanoscale*, 2018, 10 (35), pp.16521-16530. 10.1039/C8NR02267D . hal-01876308

HAL Id: hal-01876308

<https://hal.science/hal-01876308>

Submitted on 7 Nov 2019

HAL is a multi-disciplinary open access archive for the deposit and dissemination of scientific research documents, whether they are published or not. The documents may come from teaching and research institutions in France or abroad, or from public or private research centers.

L'archive ouverte pluridisciplinaire **HAL**, est destinée au dépôt et à la diffusion de documents scientifiques de niveau recherche, publiés ou non, émanant des établissements d'enseignement et de recherche français ou étrangers, des laboratoires publics ou privés.





Open Archive Toulouse Archive Ouverte (OATAO)

OATAO is an open access repository that collects the work of Toulouse researchers and makes it freely available over the web where possible

This is an author's version published in: <http://oatao.univ-toulouse.fr/24663>


Official URL: <https://doi.org/10.1039/C8NR02267D>

To cite this version:

Dong, Dongmei and Wang, Wenwen and Rougier, Aline and Dong, Guobo and Da Rocha, Mathias and Presmanes, Lionel  and Zrikem, Khawla and Song, Giljoo and Diao, Xungang and Barnabé, Antoine  *Life-cycling and uncovering cation-trapping evidence of a monolithic inorganic electrochromic device: glass/ITO/WO₃/LiTaO₃/NiO/ITO*. (2018) *Nanoscale*, 10 (35). 16521-16530. ISSN 2040-3364

Any correspondence concerning this service should be sent to the repository administrator: tech-oatao@listes-diff.inp-toulouse.fr

Life-cycling and uncovering cation-trapping evidence of a monolithic inorganic electrochromic device: glass/ITO/WO₃/LiTaO₃/NiO/ITO

Dongmei Dong,^a Wenwen Wang,^a Aline Rougier,^b Guobo Dong,^a Mathias Da Rocha,^b Lionel Presmanes,^c Khawla Zrikem,^b Giljoo Song,^b Xungang Diao ^{*a} and Antoine Barnabé^c

The visualization of the microstructure change and of the depth of lithium transport inside a monolithic ElectroChromic Device (ECD) is realized using an innovative combined approach of Focused Ion Beam (FIB), Secondary Ion Mass Spectrometry (SIMS) and Glow Discharge Optical Emission Spectroscopy (GDOES). The electrochemical and optical properties of the all-thin-film inorganic ECD glass/ITO/WO₃/LiTaO₃/NiO/ITO, deposited by magnetron sputtering, are measured by cycling voltammetry and *in situ* transmittance analysis up to 11 270 cycles. A significant degradation corresponding to a decrease in the capacity of 71% after 2500 cycles and of 94% after 11 270 cycles is reported. The depth resolved microstructure evolution within the device, investigated by cross-sectional cutting with FIB, points out a progressive densification of the NiO layer upon cycling. The existence of irreversible Li ion trapping in NiO is illustrated through the comparison of the compositional distribution of the device after various cycles 0, 100, 1000, 5000 and 11 270. SIMS and GDOES depth profiles confirm an increase in the trapped Li content in NiO as the number of cycles increases. Therefore, the combination of lithium trapping and apparent morphological densification evolution in NiO is believed to account for the degradation of the ECD properties upon long term cycling of the ECD.

DOI: 10.1039/c8nr02267d

1. Introduction

Electrochromic (EC) devices have attracted great attention during the past few decades due to their various applications in displays, automotive rearview mirrors, gas sensors, and smart windows.^{1,2} Among all device configurations, lithium ion (Li⁺) based monolithic inorganic all-thin-film layer stacks present considerable advantages regarding the production cost and commercial applications.^{3–5} A complete inorganic device with Li⁺ ions as electrochromically driven ions typically consists of a substrate coated with commercial Transparent Conducting Oxide (TCO) films for instance Indium Tin Oxide (ITO), an anodic electrochromic layer (NiO), an inorganic ion conducting layer (LiTaO₃), a cathodic electrochromic layer (WO₃), and finally another TCO electrode.⁶ NiO as an active anodic EC layer, which is complementary to the excellent cathodic EC material WO₃, shows bleaching and coloration

upon insertion and extraction of lithium ions. Li⁺ insertion is accompanied by the reversible reduction of Ni³⁺ (brown) to Ni²⁺ (transparent).

Numerous efforts in the field of inorganic ECDs have been taken to pursue even higher optical modulation and more excellent electrochemical properties or design novel configurations. Until now, studies on complete inorganic all-thin-film ECDs prepared monolithically layer by layer have been rather scarce. Patel *et al.*⁵ have reported some work on the preparation of a new inorganic all-oxide-solid-state stacked structure of ITO/Li_yWO_{3–x}/Li_{1–z}Mn₂O₄/ITO deposited on a silica glass substrate by pulsed laser deposition. Zheng-Bo Han *et al.*⁷ have focused on the pure inorganic device multi-color electrochromism based on vanadium-substituted Dawson type polyoxometalate electrochromic thin films. Tatsuo Niwa *et al.*⁸ have taken a step forward studying the response speed and temperature relevant properties of the inorganic device IrO_x/WO₃. Ullrich Steiner *et al.* have made great achievements in the research of inverse opal vanadium oxide films,⁹ enhanced electrochromism in gyroid-structured vanadium pentoxide¹⁰ and the extended application in the field of supercapacitors.¹¹ However, until now very few studies have reported on the inorganic monolithic all-thin-film device durability as

^aElectrochromic Center, School of Physics and Nuclear Energy Engineering, Beihang University, Beijing 100191, PR China. E mail: diaoxg@buaa.edu.cn

^bCNRS, Univ. Bordeaux, ICMCB, UMR 5026, F 33600 Pessac, France

^cCIRIMAT, Université de Toulouse, CNRS, Université Toulouse 3 Paul Sabatier, 118 route de Narbonne 31062, Toulouse Cedex 9, France

well as on the degradation mechanism, which plays a crucial role in EC device commercial applications. Even though Li *et al.*¹² have carried out research on the durability improvement of nanocomposite materials in a liquid electrolyte, it is still limited in a single EC layer. Sung *et al.*¹³ also reported an improvement in the durability with an inorganic protective layer for the laminated device V_2O_5/WO_3 , but organic electrolytes rather than inorganic ones were used for device lamination. Baloukas *et al.*¹⁴ have demonstrated ion trapping and detrapping limited in single EC layer WO_3 films. To the best of our knowledge, the degradation of inorganic devices has been characterized by combining chronoamperometry and voltammetry techniques,⁶ but no clear micro-mechanism has been given about the observed degradation of complete inorganic devices. Until now, for complete inorganic EC devices, no direct micro-evidence or no clear scientific explanation for capacity degradation with device long-term evolution has been found. This problem stems from the difficulty in detecting evolution inside the five-separate-layer assembly and inspecting the movement of very light lithium ions. Such a one stack device has five distinct layers and related problems associated with charge transport across any of them can have a deleterious effect on the performance. The monitoring of the internal state within a five-layer film is difficult to realize, mainly because it is hidden from view by the techniques of surface characterization. The study of electrochromism-driven lithium ion chemistry in a buried EC layer is made difficult by its lack of an Auger electron emission and its weak signal in other techniques.¹⁵ In the case of a laminated EC system, the analysis of the reaction mechanism is somewhat easier because it can be decomposed.¹⁶ In contrast to this, the analysis of monolithic all-thin-film devices is too difficult to deduce a definite conclusion.¹⁷ In summary, the lack of research on multi-layer inorganic devices' degradation mechanism is mainly due to two reasons: the inability to obtain a precise (i) elemental distribution including lithium buried beneath the surface and (ii) the detection of the micro-structure from a clear cross-section.

Driven by the difficulties in detecting lithium distribution and microstructure evolution in the EC devices, an innovative combined approach is introduced, where Scanning Electron Microscopy (SEM) coupled with Focused Ion Beam (FIB) and Glow Discharge Optical Emission Spectroscopy (GDOES) as well as Secondary Ion Mass Spectrometry (SIMS) are used to visualize the microstructure change and the depth lithium transport inside the layered device. Even if SIMS is only used as comparative elemental analysis, its excellent sensitivity to

lithium^{18–21} makes this technique a perfect candidate for the investigation of functional layers in devices. A few earlier studies tried to detect the remaining lithium by SIMS but were only limited to EC single layer WO_3 and V_2O_5 .^{22,23} This article reports an investigation of the lithium distribution in a complete monolithic inorganic device and its relationship with charge capacity fading as well as device degradation using SIMS-depth profiling. As a reference, GDOES is carried out as an independent comparative analytical technique for the lithium depth profile analysis, and to exclude potential measurement artefacts of the SIMS analysis (*e.g.* SIMS matrix effects).¹⁸ Additionally, SEM/FIB is applied advantageously to uncover the microstructure lying beneath the exposed surface, which is capable of observing a precise cross-cut section of the multilayered device. Combination of techniques is extremely useful for complete inorganic device analysis and gives us a real insight into the causes of capacity fading and durability problems of the monolithic five-layer device.

2. Experimental

2.1 Deposition of the EC device and electro-optical test

The complete inorganic all-thin-film ECD glass/ITO/ WO_3 /LiTaO₃/NiO/ITO was monolithically deposited layer by layer using magnetron sputtering at room temperature. The film stack was prepared on a commercial ITO glass substrate, with a target-to-substrate separation distance of 17 cm and the holder rotating on its symmetrical axis at a constant speed to ensure the uniformity of the films in the sputtering process. More details on the optimized device deposition parameters are gathered in Table 1. Cyclic Voltammetry (CV) experiments were carried out by using a conventional two-electrode configuration on a voltalab PG201 electrochemical workstation. ECDs after various CV cycles are labeled as ECD-fresh, ECD-100, ECD-1000, ECD-5000 and ECD-11 270 in the following. ECD-fresh is a sample in the as-deposited state, used as a reference for a pristine device without any contact with the electricity source. The optical transmittance of the films was obtained with a UV-Vis spectrometer (Evolution 100, Thermo Electron Corporation) between 300 and 800 nm.

2.2 Structural/microstructure characterization of device degradation

Raman spectroscopy was used for structural characterization. Raman spectra were collected under ambient conditions using a Horiba Jobin Yvon LabRAM HR 800 spectrometer equipped

Table 1 Detailed deposition parameters of the ECD

Order	Target	Power source	Pressure (Pa)	Ar : O ₂	Power (W)	Time (min)	Thickness (nm)
1	W	DC	2.2	27 : 9	228	10	500
2	LiTaO ₃	RF	1.0	47.5 : 2.5	153	150	200
3	Ni	DC	3.0	94 : 6	234	30	400
4	ITO	DC	0.3	99 : 1	245	20	300

with a fiber coupled 532 nm laser. Spectra acquisition was carried out for 300 s using a $\times 100$ objective lens and 600 gr mm^{-1} grating. During the measurement, the resulting laser power at the surface of the sample was adjusted to 1.7 mW. The depth of field in the Raman experimental setup is about 2.6 μm . However, the total thickness of the multilayer stacking is only 1.4 μm , and even if the optical set is focused on the surface of the sample, we can assume that the laser diameter remains the same in all the entire 5 layers. Then the focalization is not the main limitation in our case. What could limit the laser penetration in the under layers is the presence of one absorbing layer at the surface. As all the samples are observed in a bleached state in the visible part of the light spectrum (laser wavelength is 532 nm), there is no problem encountered by the various layers, and the Raman spectra show the most intense peaks of the entire stacking.

Moreover, in order to gain an insight into the microstructure situation beneath the surface, a Field Emission Gun (FEG)-SEM (JEOL JSM 7800F Prime) and FEG-SEM/FIB apparatus (FEI Helios Nanolab600i dual beam) are used to realize the Energy Dispersive Spectroscopy (EDS) elemental analysis and observation of the cross cut section of the multilayered device.

2.3 Elemental characterization of device degradation

GDOES analysis of the internal composition of the monolithic device glass/ITO/ WO_3 /LiTaO₃/NiO/ITO was performed by using

a glow discharge analyzer (HORIBA GD Profiler 2). For complementary depth profiling research on the lithium distribution, the SIMS technique was applied with a Cameca IMS-4FE6 system.

3. Results and discussion

3.1 Structure and electro-optical properties of single layers

In order to analyze the structure properties of films, X-ray diffraction (XRD) was used with a Cu K α source ($\lambda_{\text{K}\alpha 1} = 1.5405 \text{ \AA}$ and $\lambda_{\text{K}\alpha 2} = 1.5445 \text{ \AA}$) on various dedicated single and multilayer stacks. In Fig. 1a, besides the Bragg peaks corresponding to the ITO phase, no additional peaks are visible for WO_3 or LiTaO₃ when deposited on the top layer. In contrast, the XRD pattern of the NiO layer consists of two additional intense peaks corresponding to the cubic phase (space group $Fm\bar{3}m$). This suggests that in the complete device WO_3 and LiTaO₃ exist in the amorphous state, while NiO remains crystallized.

CV testing is conducted for WO_3 and NiO thin films (Fig. 1b and c) in a lithium-based electrolyte, namely lithium bis-trifluoromethanesulfonimide (LiTFSI, Solvionic, purity >99.99%) in 1-butyl-3-methylimidazoliumbis (trifluoromethanesulfonyl)-imide (BMITFSI). The cathodic EC WO_3 film has the maximum reduction current density of -0.86 mA cm^{-2} at -1 V and the maximum oxidation current density of $+0.65 \text{ mA cm}^{-2}$ at -0.25 V . The anodic EC NiO film has the maximum oxidation current density of $+0.195 \text{ mA cm}^{-2}$ at $+0.78 \text{ V}$ and

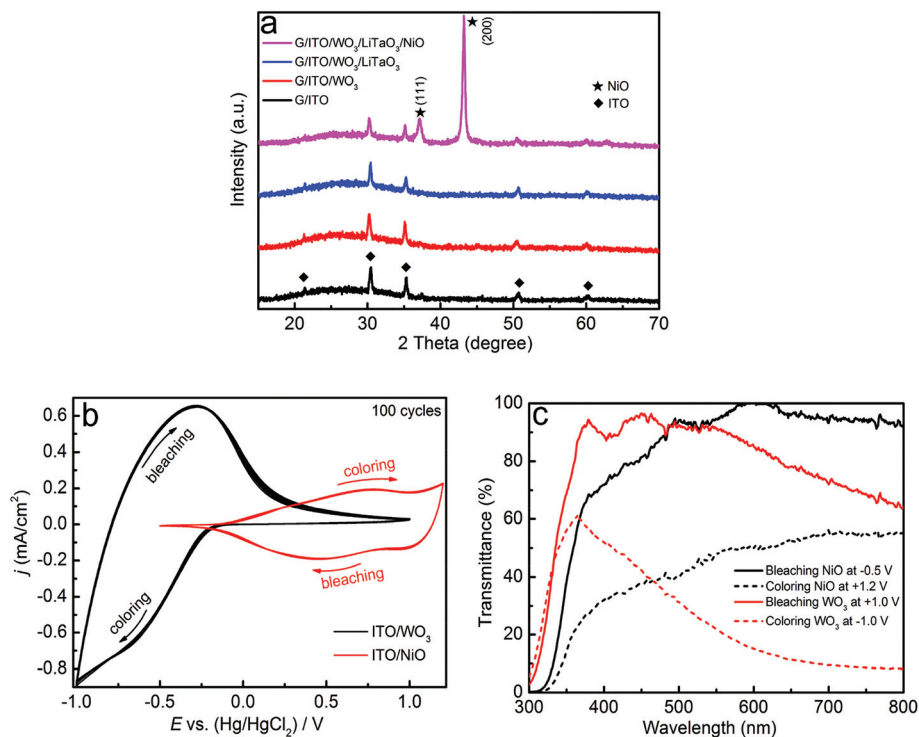


Fig. 1 (a) XRD patterns of films, glass/ITO, glass/ITO/ WO_3 , glass/ITO/ WO_3 /LiTaO₃ and glass/ITO/ WO_3 /LiTaO₃/NiO deposited for the complete ECD glass/ITO/ WO_3 /LiTaO₃/NiO/ITO. (b) CV curve of EC NiO and WO_3 films cycling in 1 M LiTFSI BMITFSI electrolyte with a scan rate of 40 mV s^{-1} and (c) their corresponding transmittance spectra.

Table 2 Bleached/colored transmittance, optical density, charge capacity and coloration efficiency at the wavelength 550 nm for NiO and WO₃ films

EC films	T_b (%)	T_c (%)	ΔOD	Q (C m ⁻²)	η (cm ² C ⁻¹)
NiO	94	47	0.30	45	66.7
WO ₃	91	21	0.64	127	50.4

two obvious reduction peak current densities of -0.14 and -0.19 mA cm⁻² at $+0.96$ and $+0.44$ V, respectively. The WO₃ film has a higher reaction current density and calculated charge capacity than NiO; however, as presented in Table 2, NiO has a higher coloration efficiency (η). It indicates that charges within NiO are more efficient for electrochromism behavior. η is a crucial parameter to judge an EC film which represents the change in the optical contrast (ΔOD) for the charge consumed per unit of electrode area (Q).^{8,24} It can be evaluated from the formula:

$$\eta = \Delta OD / Q = \log(T_b / T_c) / Q,$$

where T_b and T_c are the bleaching and colored transmittance at the wavelength 550 nm, respectively. The corresponding potentials are listed in Fig. 1(c).

3.2 Electro-optical properties of complete device ITO/WO₃/LiTaO₃/NiO/ITO

The FEG-SEM cross-sectional image of ECD-fresh unambiguously presents a five-layered ITO/WO₃/LiTaO₃/NiO/ITO configuration with no interfacial contamination within the detection limit of the technique (Fig. 2). EDS element maps are used to provide complete composition distribution analyses of the complete inorganic ECD: glass/ITO/WO₃/LiTaO₃/NiO/ITO. As expected, the element “In” from ITO electrodes is scattering in the scope of top and bottom layers. The middle layer LiTaO₃ electrolyte is evidenced by the distribution range of element “Ta”. Li is less evidenced due to its low atomic number which

induces a low yield and low energy of the characteristic X-rays. Electrochromic films WO₃ and NiO are as designed on the two sides of LiTaO₃. The compositional uniformity and the sharp interfaces between layers indicate that the complete inorganic all-thin-film device is fabricated successfully by the monolithic preparation method.

The stability of the device is usually associated with electrochemical stability since the degradation of the charge capacity results in a loss of EC contrast and hence the behavior of the EC device.²⁵ To study the dynamics of charge density exchange of the complete cell device, we conducted long-term voltammetric cycling for more than 11 000 cycles with the potential ranging from -1.6 to 0.5 V and the scan rate set at 40 mV s⁻¹ (Fig. 3). For the purpose of studying the lithium distribution dynamics in the cycling process, voltammetry profiles with various cycles are performed onto the five devices named ECD-fresh, ECD-100, ECD-1000, ECD-5000 and ECD-11 270. Upon cycling, the decrease in the area cycled for consecutive CV curves indicates that fewer charges are able to move within the device corresponding to a degradation of the EC performance. The *in situ* transmittance evolution for some chosen cycles is shown in Fig. 4. Both the coloration and bleaching transmittances increase with time. The device becomes less and less colored, suggesting the progressive decrease in the Ni³⁺ (brownish) or W⁵⁺ (blue) ion content. The colored state changes from dark to light brownish, while the bleached state is getting more and more transparent upon long-term cycling. In general, the basic degradation of devices results from the decline in the contrast ratio induced by a decreased transmittance in the bleached state, an increased transmittance in the colored state or a combination of both.²⁶ Herein, for the monolithic inorganic device glass/ITO/WO₃/LiTaO₃/NiO/ITO, the inability to get a deep coloration is the main factor contributing to the device decline in the long-term optical switching process. Interestingly, the charge capacity of the fresh device (Fig. 3b) is near 40 C m⁻², surprisingly, approaching to the capacity of 45 C m⁻² for anodic NiO (shown in Table 2) as

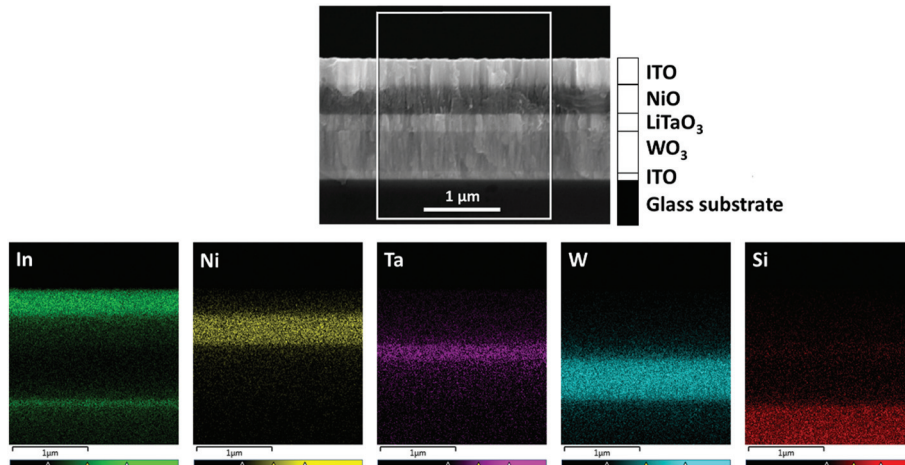


Fig. 2 SEM cross sectional image and EDS elemental maps of ECD fresh: glass/ITO/WO₃/LiTaO₃/NiO/ITO.

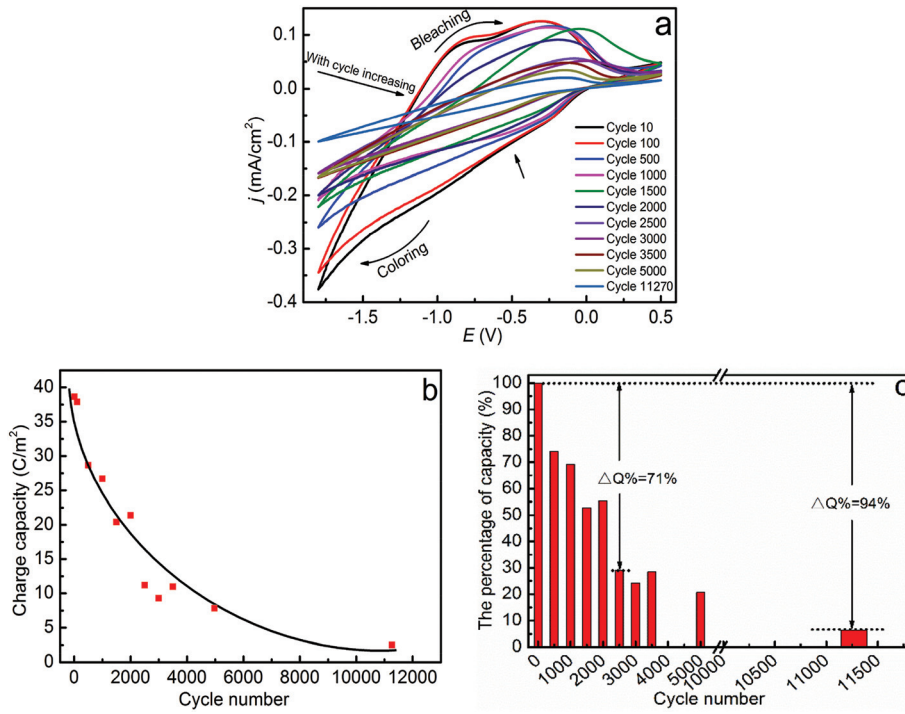


Fig. 3 Typical cyclic voltammogram (a) of the device glass/ITO/WO₃/LiTaO₃/NiO/ITO scanned at a rate of 40 mV s⁻¹ and the corresponding charge capacity (b) and the percentage of decaying capacity upon cycling (c).

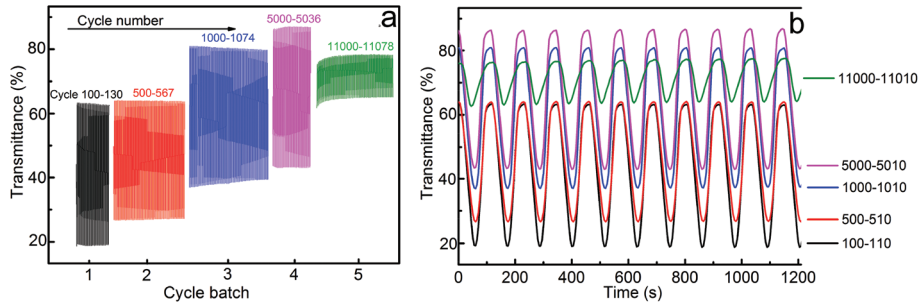


Fig. 4 (a) *In situ* transmittance evolution of the EC device glass/ITO/WO₃/LiTaO₃/NiO/ITO and (b) detailed enlargement for 100–110, 500–510, 1000–1010, 5000–5010, and 11000–11010 cycle ranges.

earlier discussed by Da Rocha *et al.*²⁷ Indeed, the complete device capacity is mostly governed by the EC layer with a smaller capacity, usually, the NiO layer. Taking the very first cycle as 100% capacity (Fig. 3c), the device exhibits a 71% sharp decrease in 2500 cycles and a 94% drop in 11 270 cycles, showing a rapid initial drop followed by a very gradual decline of the charge density as the cycle number progresses.

3.3 Structural/microstructure analysis of ITO/WO₃/LiTaO₃/NiO/ITO device degradation

Due to the low penetration depth of X-rays and the large thickness of the top ITO layer (300 nm), X-ray-diffraction is not efficient to structurally characterize the NiO layer of the complete ECD after various cycling times. As a result, visible photons ($\lambda = 532$ nm) involved in Raman spectroscopy are

used to structurally monitor the potential device degradation. The Raman spectra of the complete device glass/ITO/WO₃/LiTaO₃/NiO/ITO show mainly three vibration bands in the range of 100–1700 cm⁻¹ (Fig. 5). By comparison with the pure thin films deposited on ITO glass, the peak centered at 510 cm⁻¹ is related to NiO and another two centered at 800 and 958 cm⁻¹ are assigned to WO₃. For reference purposes, all cycles start from the initial potential 0 V and end at the final 0 V, corresponding to a non-colored and non-bleached state. That is to say, all Raman spectra correspond to films in the same state after cycling; as shown in Fig. 5b, except for the NiO peak in the fresh sample, we do not see any clear regular shift from fresh to 11 270 cycles. There is no visible change in the WO₃ sample too. This suggests that the electro-optical degraded device still maintains the macro-scale structure-stabi-

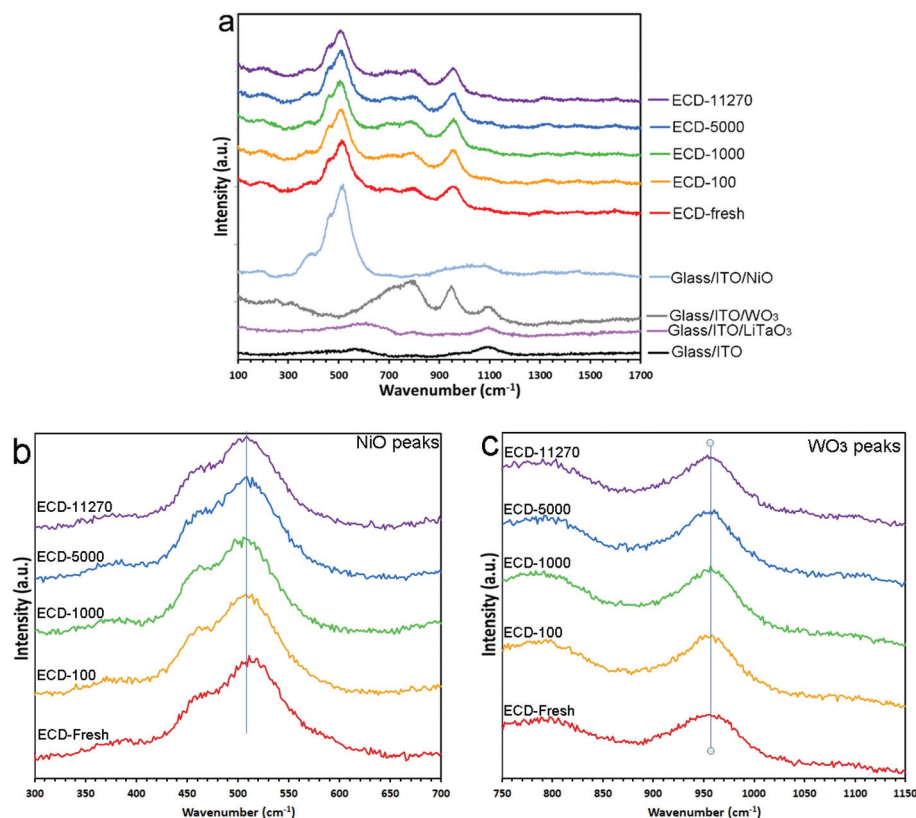


Fig. 5 (a) Raman spectra of the device glass/ITO/WO₃/LiTaO₃/NiO/ITO after various cycles, and partial enlargement of (b) NiO and (c) WO₃ peaks.

lity. This leads to the question on which sites the reactions take place and where do the trapped ions remain in the films? It is a debated question that remains unsolved. In one review article Niklasson and C. G. Granqvist²⁸ pointed out that the electrochromism is basically a surface effect/phenomenon and argued that the change of the NiO to Ni₂O₃ may occur at the interface, while the bulk remains NiO independently of the film being bleached or colored. This could explain to some degree why similar vibration modes are obtained in films after various cycles.

We investigate the microstructures by FEG/SEM (Fig. 6). For subsequent imaging *via* SEM, FIB was used to create a very precise cross-section of each sample without any mechanical stress and/or contaminants like grinding/polishing slurries. Despite the artefacts of amorphization of the ITO, LiTaO₃ and WO₃ outer layers, Ga implantation and low curtaining of the bottom layers, NiO layer cross-section parts are well evidenced by this preparation technique. The image contrast of the device after long-term cycling and the as-deposited ones comes from the porosity and empty volumes just in the NiO domain. More specifically, SEM/FIB imaging shows that the porosity of the NiO layer is strongly affected by the cycling behavior with a significant decrease in the number of the empty volumes from 0 to 5000 cycles. In comparison with the as-deposited and degraded devices, great morphological changes are observed in the NiO region. It can be seen that the NiO

film is composed of nanoparticles with a tiny and uniform particle size as well as porous space, the feature can allow ions in the electrolyte to penetrate through the films freely and shorten their diffusion paths in the films. The multi-cycling has led to a smoother and denser morphology for NiO until 5000 cycles.

However, it is an apparently different case for the ECD after 11 270 cycles (ECD-11 270). Extremely long-time voltammetric cycling has caused the partial separation of WO₃ and LiTaO₃ layers, thus creating some cracks at their interface. Additionally, on the planar view, *i.e.* on the top ITO electrode, some “micro-holes” indicated as black dots appear between ITO particles, suggesting the electrode decohesion. Accompanying the appearance of such holes at the particle interface, great changes also take place within ITO particles, causing the dissolution of uniformly distributed grains. Based on the evolution mentioned above, for ECD-11 270, the NiO layer dramatically transforms to an even more disorder porous state, combined with the electrode decohesion, thus hindering the movement of ions and charges and depressing the charge capacity. It should be stressed that the main information we get from Fig. 6e is the decohesion between the WO₃ and LiTaO₃ and “holes” from the top surface of the ITO electrode. These new phenomena in ECD-11 270 may be associated with the dramatic change and degradation. We would not insist on the porosity evolution of the NiO layer for ECD-11 270. In this

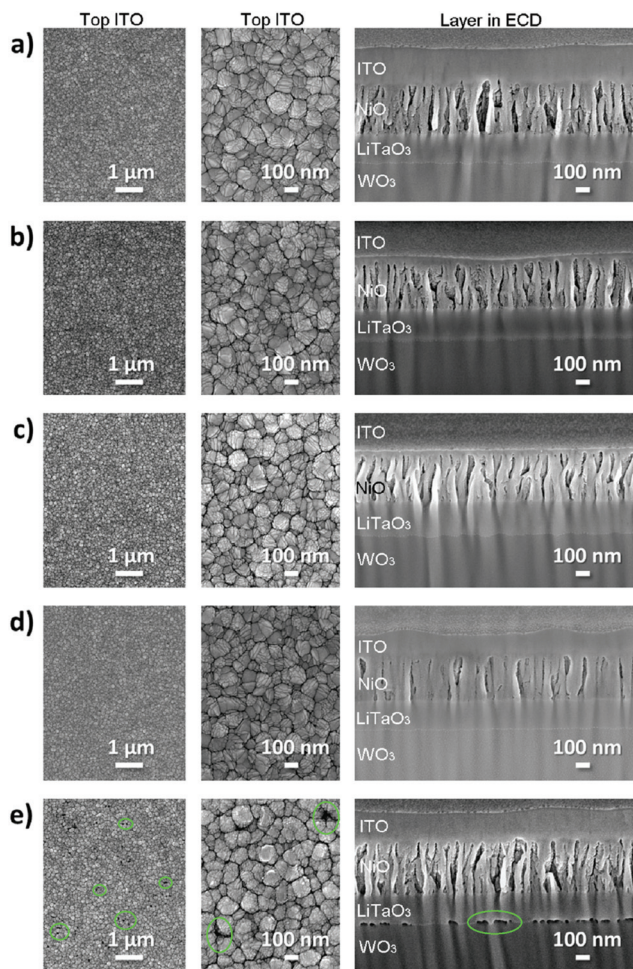


Fig. 6 SEM top view morphology image of the ITO surface and SEM cross sectional view image of the ECDs (a) ECD fresh; (b) ECD 100; (c) ECD 1000; (d) ECD 5000; (e) ECD 11270. To make it clear, micro changes ("holes" and decohesion) are marked with green circles.

work, the depth resolved microstructure evolution within the device is investigated by the cross-sectional cutting with SEM/FIB and a densifying tendency is observed in the NiO layer upon 5000 cycles. As this is the first report on inorganic monolithic all-thin-film device degradation by the combination of SEM/FIB, GDOES and SIMS, in the beginning we focused our attention on the microstructure evolution and Li^+ trapping issue and more precisely on the electrochromic NiO layer which is not fully studied. The NiO within the complete device, not like the single layer, is not only affected by repeated voltammetric cycling, but also by other factors such as interactions between different films and the evolution of the other layers (the appearance of delamination or electrode "holes"). Here, the new decohesion and holes may have connections to the dramatic porosity change in ECD-11270, but there still remains a number of unknowns and further study is needed. Indeed, the systematic study of the inorganic monolithic all-thin-film device is of great interest and is necessary to fully understand the electrochromic degradation mechanism.

3.4 Elemental analysis of ITO/ WO_3 /LiTaO₃/NiO/ITO device degradation

As a key criterion, the memory effect, which is defined as the ability to retain the lithium ions in the EC layer as well as maintain the transmittance value after the potential is removed, was characterized. The five-layer monolithic inorganic device does not show a good memory effect, associated with an obvious self-erasing process taking place in the device under open-circuit conditions.

The fresh device and ECDs after different life-cyclings, 100, 1000, 5000, and 11270 cycles (Fig. 7), are characterized by GDOES and SIMS techniques. To find out the composition change including lithium distribution, depth profiling has been conducted. Unexpectedly, in the fresh uncycled device, a significant lithium content appears in the WO_3 layer. As the quantitative analysis could not be carried out without identical matrix and charging effects, it is not possible to quantify this lithium quantity. However, within the same layer, *i.e.* with the constant matrix and charging effect, both SIMS and GDOES analyses allow for comparison for a given one element. According to the literature, some studies have reported that for the deposition process of the monolithic all-thin-film ECD, it is possible for the depositing layer to interact with the deposited layers.²⁹ Here, the deposited layer refers to WO_3 and the depositing one to LiTaO₃. In the plasma process, the electrical fields on or near the exposed film surface generated by electrons and plasma ions will cause the lithium ions to migrate within the EC layers. In the specific case of the inorganic lithium containing electrolyte deposition process, Widjaja *et al.*³⁰ have discovered the lithium ion insertion on top of a WO_{3+x} super-stoichiometric layer. For our device, it can be concluded that there is also lithium migration into WO_3 films during the deposition process of the electrolyte LiTaO₃ layer. Furthermore, the lithium concentration in the WO_3 region remains at a high level for the fresh device (shown in Fig. 7).

The GDOES depth profiles for the different samples ECD-fresh, ECD-100, ECD-1000 and ECD-5000 with the above cycling histories are depicted in Fig. 7a. Overall, a homogeneous elemental distribution of Ni, Ta and W is detected in NiO, LiTaO₃ and WO_3 layers, respectively. Moreover, a higher intensity in the "In" signal at the interface ITO/NiO arises from the strong interfacial effect; the sharpness of the increase in the bottom ITO region is a result of the GDOES artefacts. Upon long-term cycling, the Li distribution is significantly changed. As shown in the zoom of GDOES analysis of Li, the signal exhibits a much higher intensity in the anodic NiO layer for the sample ECD-5000. Conversely, this device has a decreased Li intensity for the cathodic WO_3 layer. Compared to the significant change of the Li level for devices after 5000 cycles, the difference of other samples before 1000 cycles is less pronounced that may be caused by the testing and it does not make sense for further discussion. The GDOES analysis demonstrates that extensive voltammetric cycling mainly results in the irreversible Li trapping in the NiO layer, thus

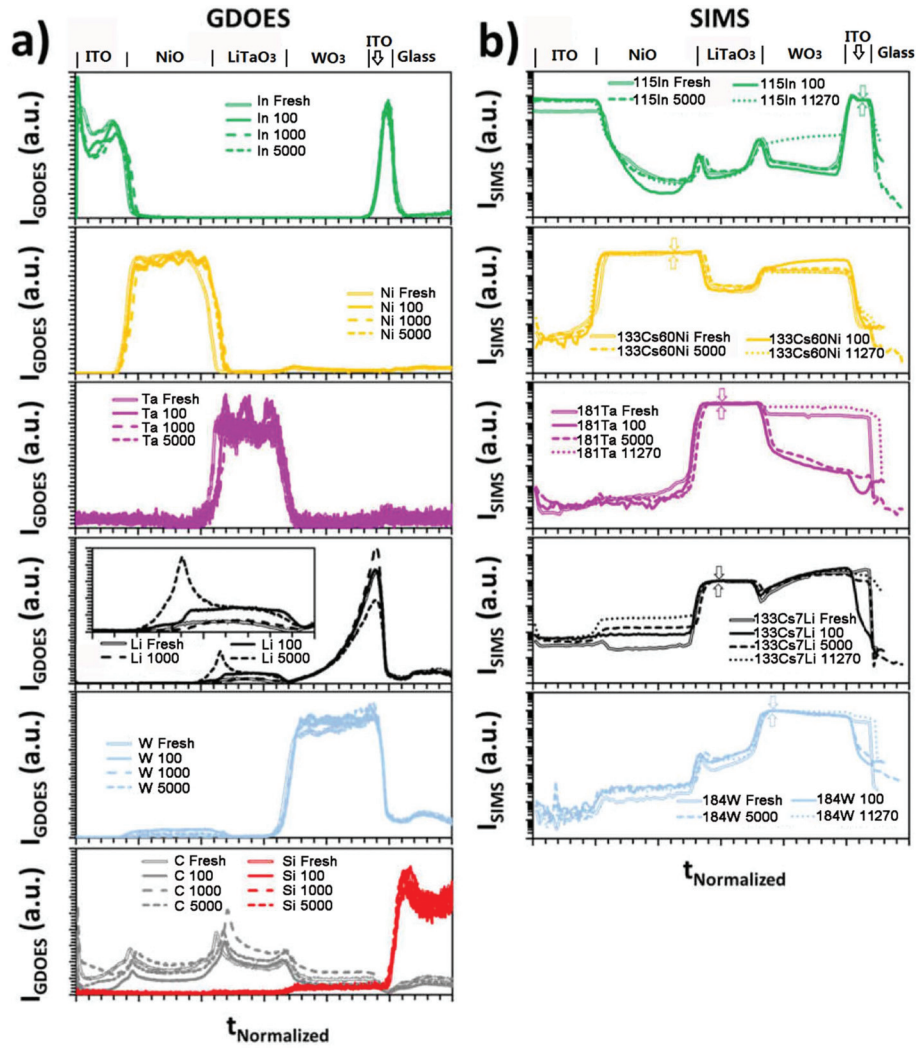


Fig. 7 (a) GDOES profiles of ECD: ITO/NiO/LiTaO₃/WO₃/ITO/G after 0 (fresh), 100, 1000 and 5000 cycles and (b) SIMS profiles after 0 (fresh), 100, 5000 and 11270 cycles. The inset figure is a zoom of Li spectra. SIMS intensity is normalized depending on the analyzed element and it is marked with a double arrow. All the intensities and time scales are normalized in order to compare the different ECDs.

restraining the charge density exchange. The trapped Li ions in the NiO film theoretically help generate more Ni²⁺ ions and make the device less colored, and the deduction is in good agreement with the experimental transmittance data (Fig. 4).

For complementary depth profiling results on the elemental distribution, SIMS measurements have been carried out as a comparative analytical technique and the samples ECD-fresh, ECD-100, ECD-5000 and ECD-11270 have been analyzed. The SIMS depth profiles of the negative secondary ions for the devices are shown in the log scale in Fig. 7b. The elemental distribution of In, Ni, Ta, Li and W within the device is visualized by ¹¹⁵In, ¹³³Cs⁶⁰Ni, ¹⁸¹Ta, ¹³³Cs⁷Li and ¹⁸⁴W mass signals, respectively. The results are also used to further confirm the increased Li concentration in the NiO layer upon long-term cycling. Panel b shows the SIMS depth profile of ECDs with the same cycling history as the GDOES analysis in panel a. The Li signal in the NiO film shows an unambiguous higher Li content with an increase in the cycle number, which is further

evidence that Li trapping does take place in the NiO layer and consistent with the analog GDOES results. The In, Ni, Ta and W signals are homogeneous within their corresponding layers ITO, NiO, LiTaO₃ and WO₃, but exhibit some insignificant steps across different layers in the complete device since it is sensitive to matrix effects (due to the spatial separation of the sputter and the excitation process in SIMS characterization).³¹ Some changes of intensities arise from the change in the matrix when passing from one layer to another one. For instance, it is believed that Ni has the highest concentration in the NiO layer, but the difference of the Ni content in the LiTaO₃ and WO₃ layers is insignificant. In addition to the ITO layer, the other layers also show “In” intensity as well. This “migration illusion” is induced by SIMS measurement artefacts. The SIMS intensity will always be measurable even when the element is in infinitesimal proportion in the matrix, and it is enlarged by the log scale here. At the same time, the GDOES technique, where the matrix effect is insignificant in this

measurement, does not give “In” intensity in other layers. This explains why a residual “In” SIMS intensity could be measured in the NiO, LaTiO₃ and WO₃ layers. It is known also that the matrix effect could be very important and often give rise to an intensity increase at the interface. The same behavior is observed for the W SIMS intensity at the NiO/LaTiO₃ interface. For this point, it is interesting to compare these values with the GDOES results where this matrix effect is not present. It is noteworthy that, in SIMS observation, Li in WO₃ seems to be not very affected by cycling (no clear tendency), but both SIMS and GDOES without any doubt prove that there is a large amount of Li inside the WO₃ layer in all the samples. This must be correlated with the deposition process (see the fresh sample) and the explanation is given above.

Despite their own measurement artefacts, namely, GDOES: a sharp increase at the interface and SIMS: the intensity influenced by the matrix effect, the innovative combination of the two analytical methods can yield a qualitative description of the elemental composition. For the NiO layer, the more cycles are iterated, the more the remaining lithium concentration is. This is direct proof that the ions trapped in NiO participate in the decrease of the charge capacity from electrochemical cycling and in the ECD degradation. It is known that the lithium ion insertion into the anodic NiO layer is associated with a reduction of Ni³⁺ (brownish) to Ni²⁺ (transparent).¹⁷ Thus the irreversible trapped lithium ions in NiO contribute to an increase in the transmittance in the bleached state associated with a less-colored state for the complete device if opposite-direction electricity is applied. Such an observation agrees well with the optical switching presented in Fig. 4 up to 5000 cycles while for extended cycling (11 270) other additional phenomena such as film decohesion take place.

4 Conclusion

We have reported in this paper that the monolithic device glass/ITO/WO₃/LiTaO₃/NiO/ITO degradation mechanism lies in lithium trapping issues in the NiO layer as well as the appearance of “micro-holes” in the top ITO electrode and decohesion between LiTaO₃ and WO₃ layers. From the Raman spectra of the device after long-term cycling endurance for more than 11 000 cycles, it was found that the capacity degraded device has an unchanged film macro-structure. In order to give a clear explanation about the capacity fading and degradation basic reasons, the state of the Li distribution was investigated by depth profiling *via* GDOES and SIMS. Both techniques independently revealed a higher irreversible Li content in the NiO region upon device long-term cycling. In combination with structural characterization including Raman and SEM/FIB analyses, it is reckoned that the inorganic device degradation mechanism comes from the evolving micro-structure of the NiO layer and related lithium trapping only limited in this layer. The FIB method was employed for the imaging of micro-structures in the device and it was found that the densification occurs in NiO films upon cycling for 5000 cycles and the evol-

ution is even more complex after 11 270 cycles considering the electrode disruption. The FIB-cut image analysis also disclosed a significant microstructure change arising from the irreversible lithium trapping in the NiO layer with cycling. This lithium trapping along with apparent morphology evolution in the NiO domain is believed to account for the charge density exchange decline in the complete inorganic device glass/ITO/WO₃/LiTaO₃/NiO/ITO.

Conflicts of interest

There are no conflicts to declare.

Acknowledgements

This work was financially supported by the National Program on Key Research Project (2016YFB0303900) and the Academic Excellence Foundation of BUAA for PhD Students (2017062). The authors acknowledge T. Hungria and C. Josse from the Microcharacterization Centre Raimond Castaing (UMS3623), Université de Toulouse for providing the SIMS and SEM/FIB characterization of the devices.

References

- 1 C. G. Granqvist, E. Avendaño and A. Azens, *Thin Solid Films*, 2003, **442**, 201–211.
- 2 S. Poongodi, P. S. Kumar, D. Mangalaraj, N. Ponpandian, P. Meena, Y. Masuda and C. Lee, *J. Alloys Compd.*, 2017, **719**, 71–81.
- 3 S. I. Park, S. Kim, J. O. Choi, J. H. Song, M. Taya and S. H. Ahn, *Thin Solid Films*, 2015, **589**, 412–418.
- 4 D. Y. Ma and J. M. Wang, *Sci. China: Chem.*, 2017, **60**, 54–62.
- 5 K. J. Patel, G. G. Bhatt, J. R. Ray, P. Suryavanshi and C. J. Panchal, *J. Solid State Electrochem.*, 2017, **21**, 337–347.
- 6 C. Person, I. Porqueras, M. Vives, C. Corbella, A. Pinyol and E. Bertran, *Solid State Ionics*, 2003, **165**, 73–80.
- 7 L. Liu, S. M. Wang, C. Li, C. G. Liu, C. L. Maa and Z. B. Han, *Pure Inorganic, J. Mater. Chem. C*, 2015, **3**, 5175.
- 8 T. Niwa and O. Takai, *Thin Solid Films*, 2010, **518**, 1722–1727.
- 9 L. Li, U. Steiner and S. Mahajan, *J. Mater. Chem.*, 2010, **20**, 7131–7134.
- 10 M. R. J. Scherer, L. Li, P. M. S. Cunha, O. A. Scherman and U. Steiner, *Adv. Mater.*, 2012, **24**, 1217–1221.
- 11 D. Wei, M. R. J. Scherer, C. Bower, P. Andrew, T. Ryhänen and U. Steiner, *Nano Lett.*, 2012, **12**, 1857–1862.
- 12 C. P. Li, R. C. Tenent, A. C. Dillonb, R. M. Morrisha and C. A. Wolden, *ECS Electrochem. Lett.*, 2012, **1**, H24–H27.
- 13 S. J. Yoo, J. W. Lim and Y. E. Sung, *Sol. Energy Mater. Sol. Cells*, 2006, **90**, 477–484.
- 14 B. Baloukas, M. A. Arvizu, R. T. Wen, G. A. Niklasson, C. G. Granqvist, R. Vernhes, J. E. Klemberg-Sapieha and

- L. Martinu, *ACS Appl. Mater. Interfaces*, 2017, **9**, 16995–17001.
- 15 J. E. Castle, F. Decker, A. M. Salvi, F. A. Martin, F. Donsanti, N. Ibris and D. Alamarguy, *Surf. Interface Anal.*, 2008, **40**, 746–750.
- 16 J. Nagai, G. D. McMeeking and Y. Saitoh, *Sol. Energy Mater. Sol. Cells*, 1999, **56**, 309–319.
- 17 C. Dellen, H. G. Gehrke, S. Möller, C. L. Tsai, U. Breuer, S. Uhlenbruck, O. Guillon, M. Finsterbusch and M. Bram, *J. Power Sources*, 2016, **321**, 241–247.
- 18 D. Alamarguy, J. E. Castle, M. Liberatore and F. Decker, *Surf. Interface Anal.*, 2006, **38**, 801–804.
- 19 R. Janski, M. Fugger, M. Sternad and M. Wilkening, *ECS Trans.*, 2014, **62**, 247–253.
- 20 C. Pereira-Nabais, J. Światowska, M. Rosso, F. Ozanam, A. Seyeux, A. Gohier, P. Tran-Van, M. Cassir and P. Marcus, *ACS Appl. Mater. Interfaces*, 2014, **6**, 13023–13033.
- 21 T. Sui, B. Song, J. Dluhos, L. Lu and A. M. Korsunsky, *Nano Energy*, 2015, **17**, 254–260.
- 22 C. Y. Kim, S. G. Cho and T. Y. Lim, *Sol. Energy Mater. Sol. Cells*, 2009, **93**, 2056–2061.
- 23 F. Decker, F. Donsanti, A. M. Salvi, N. Ibris, J. E. Castle, F. Martin, D. Alamarguy, A. S. Vuk, B. Orelid and A. Lourenco, *J. Braz. Chem. Soc.*, 2008, **19**, 667–671.
- 24 Z. Xie, L. Gao, B. Liang, X. Wang, G. Chen, Z. Liu and G. Shen, *J. Mater. Chem.*, 2012, **22**, 19904–19910.
- 25 B. Xue, J. Peng, Z. F. Xin, Y. M. Kong, L. Li and B. Li, *J. Mater. Chem.*, 2005, **15**, 4793–4798.
- 26 C. E. Tracy, J. G. Zhang, D. K. Benson, A. W. Czanderna and S. K. Deb, *Electrochim. Acta*, 1999, **44**, 3195–3202.
- 27 M. Da Rocha, Y. He, X. Diao and A. Rougier, *Sol. Energy Mater. Sol. Cells*, 2018, **177**, 57–65.
- 28 G. A. Niklasson and C. G. Granqvist, *J. Mater. Chem.*, 2007, **17**, 127–156.
- 29 S. Oukassi, C. Giroud-Garampon, C. Dubarr, C. Ducros and R. Salot, *Sol. Energy Mater. Sol. Cells*, 2016, **145**, 2–7.
- 30 E. Widjaja and G. Delporte, Method of Making an Ion Switching Device Without a Separate Lithiation Step, *US Patent* 7830585, 2010.
- 31 K. Shimizu, H. Habazaki, P. Skeldon and G. E. Thompson, *Spectrochim. Acta, Part B*, 2003, **58**, 1573–1583.